CI&CEQ

Available on line at
Association of the Chemical Engineers of Serbia *AChE*
www.ache.org.rs/CICEQ

Chemical Industry & Chemical Engineering Quarterly 18 (3) 385–398 (2012) CI&CEQ

REZA ABEDINI[1,2]
SEYED MAHMOUD MOUSAVI[2]
REZA AMINZADEH[1,2]

[1]Research Center of Membrane Processes and Membrane, Ferdowsi University of Mashhad, Mashhad, Iran
[2]Department of Chemical Engineering, Faculty of Engineering, Ferdowsi University of Mashhad, Mashhad, Iran

SCIENTIFIC PAPER

UDC 661.882:66:678

DOI 10.2298/CICEQ111202014A

EFFECT OF SONOCHEMICAL SYNTHESIZED TIO_2 NANOPARTICLES AND COAGULATION BATH TEMPERATURE ON MORPHOLOGY, THERMAL STABILITY AND PURE WATER FLUX OF ASYMMETRIC CELLULOSE ACETATE NANOCOMPOSITE MEMBRANES PREPARED *VIA* PHASE INVERSION METHOD

In this study, asymmetric pure CA and CA/ TiO_2 nanocomposite membranes were prepared via phase inversion by dispersing TiO_2 nanoparticles in the CA casting solutions induced by immersion precipitation in water coagulation bath. TiO_2 nanoparticles, which were synthesized by the sonochemical method, were added into the casting solution at different concentrations. Effects of TiO_2 nanoparticles concentration (0, 5, 10, 15, 20 and 25 mass%) and coagulation bath temperature (CBT, 25, 50 and 75 °C) on morphology, thermal stability and pure water flux (PWF) of the prepared membranes were studied and discussed. Increasing TiO_2 concentration in the casting solution film along with higher CBT resulted in increasing the membrane thickness, water content (WC), membrane porosity and pure water flux (PWF). Also, these changes facilitate macrovoids formation. Thermal gravimetric analysis (TGA) shows that thermal stability of the nanocomposite membranes was improved by the addition of TiO_2 nanoparticles. Furthermore, TGA results indicated that increasing CBT in each TiO_2 concentration leads to the decreasing of decomposition temperature (T_d) of nanocomposite membranes.

Keywords: nanocomposite membrane; cellulose acetate; TiO_2 nanoparticles; phase inversion; coagulation bath temperature.

Nowadays membrane processes are required for a wide spectrum of separations including supply of high-quality water for domestic and industrial demands to obtain high-grade products and removal or recovery of toxic or valuable components from various industrial effluents [1-4]. The phase inversion process induced by immersion precipitation is an illustrious technique to prepare asymmetric polymeric membranes [5-10]. In this technique, a cast film containing a polymer and its appropriate solvent is immersed into a coagulation bath containing a non-solvent (material with high and low affinity to the solvent and the polymer, respectively). Then precipitation starts due to the low miscibility between the polymer and the non-solvent. Simultaneously, the high miscibility between the solvent and the non-solvent causes their diffusional flow (the exchange of solvent and non-solvent) in several points of the film top layer and the film sublayer which subsequently leads to formation of nuclei of polymer-poor phase. In fact, the low affinity between polymer chains and water molecules, at points that water molecules diffuse, results in repelling of the polymer chains and consequently formation of nuclei of polymer-poor phase. Due to continuation of the diffusional flow of solvent and non-solvent, the mentioned nuclei continue to grow until the polymer concentration at their boundaries becomes too high so that solidification occurs (demixing process completes) [2,5].

Correspondening author: R. Abedini, Department of Chemical Engineering, Faculty of Engineering, Ferdowsi University of Mashhad, P.O. Box 91775-1111, Azadi Square, Vakil-Abad Boulevard, Mashhad, Iran.
E-mail: reza.abedini20@gmail.com
Paper received: 2 December, 2011
Paper revised: 22 February, 2012
Paper accepted: 29 February, 2012

A wide range of parameters have been checked concerning the membrane formation mechanism and consequently the membrane morphology and permeability such as polymer concentration in casting solution [11], type of solvent/non-solvent pair [12], cast film thickness [13], presence of certain additives [14], coagulation bath temperature [15], addition of nanoparticles [16] and presence of some other solvents [17]. It seems that the above parameters have significant effects on the instantaneous/delayed demixing process that takes place in the coagulation bath during the membrane formation process.

Nanocomposite membranes are formed by the addition of inorganic oxide particles in micrometer as well as nanometer sizes to the polymeric casting solution or by *in situ* generation. Over the past few years, such types of membranes have received much interest in the relevant membrane processes such as reverse osmosis [18], pervaporation [19], ultrafiltration [20] and nanofiltration [21]. Few researchers have investigated the blend of organic polymer with inorganic materials like alumina, titania, silica, etc. [22-24].

Among different metal oxide nanoparticles, TiO_2 had received the most attention because of its stability, availability, and promise for applications such as medicine [25], catalysis and photocatalysis [26,27], battery [28] etc. Hence, it is of great importance to improve the preparation method of nanocrystalline TiO_2. Up to now, the methods for preparing nanometer TiO_2 can be summarized as follows: sol-gel method [29], vapor decomposition of titanium alkyloxides or $TiCl_4$ in oxygen [30], hydrothermal technique [31], reversed micelle method [32], and oxidation of metallic Ti powder [33]. Sonochemistry, by which influential ultrasound is used to inspire chemical processes in liquids, is currently the focus in a wide range of chemical materials science and technology, since it causes novel chemical reactions and physical changes which do not occur unless sonically inspired. Now, different nanostructured oxides can all be prepared by using high-intensive ultrasound [34]. As a result, ultrasonic assisted-method can be desirable for synthesis of different kinds of metal oxides such as TiO_2, SiO_2, Al_2O_3 and CuO.

In the present study, TiO_2 nanoparticles were first synthesized *via* sonochemical methods. Then, TiO_2 nanoparticles were added at concentrations from 5 to 25 mass% to the casting solution. Each casting solution was immersed in three coagulation baths at temperatures of 25, 50 and 75 °C to prepare new CA/TiO_2 composite membranes. Effects of TiO_2 nanoparticles and coagulation baths temperature on prepared membranes were investigated by SEM, XRD, TGA, WC, membrane porosity, membrane mean pore diameter and PWF tests.

MATERIALS AND METHODS

Materials

Tetraisopropyl titanate (TIPT) with analytical purity of 99.5% (Merck), ethanol (analytical grade, Merck) and de-ionized water were used without additional purification for synthesis of TiO_2 nanoparticles. CA with an average molecular weight of 30,000 g/mol (Aldrich) was used as the polymer forming membrane. The solvent used was 1-methyl-2-pyrrolidone (NMP) with an analytical purity of 99.5% (Merck). Distilled water was used as the non-solvent agent.

Synthesis of TiO_2 nanoparticles

TiO_2 nanoparticles were synthesized by the hydrolysis of tetraisopropyl titanate (TIPT) in the presence of de-ionized water, ethanol, and acetic acid as a dispersant under ultrasonic irradiation (24 kHz, 300 W/cm^2). In a typical synthesis, 150 ml of de-ionized water mixed with acetic acid (0.15 ml) and sonicated in a sonication cell. Then a mixture of TIPT and ethanol was injected drop-wise into the aqueous solution in 3 min. The water-to-TIPT and water-to-ethanol ratios were 75 and 25, respectively. The mixture was sonicated continuously under ambient air for 3 h. The sonication was conducted without cooling so that the temperature was raised from 25 to 78 °C at the reaction end. The obtained precipitates were separated by centrifugation (12,000 rpm in 30 min) and washed with de-ionized water and ethanol several times. The product was dried at 60 °C for 24 h.

Membrane preparation

CA/TiO_2 flat sheet membranes were prepared by the phase inversion method. Figure 1 shows membrane formation process in the coagulation bath. A casting solution was prepared by the addition and dispersion of TiO_2 nanoparticles in NMP, then dissolving the CA (17.5 mass%, by weight of the solution) in the mixture at room temperature. For the nanocomposite membranes (CA/TiO_2), at first TiO_2 nanoparticles were mixed with NMP and stirred for 4 h to ensure homogeneous spread of the nanoparticles. The mixture was sonicated for 5 min in a sonication cell. Then CA was added to the initial mixture in three 30-min intervals and dissolved in the solvent. Special care was taken to ensure the homogeneous dispersion of the TiO_2 nanoparticles. The concentration of TiO_2 added to CA was varied from 0 to 25 mass%. Table 1 shows the composition and CBT for each solution. In order to obtain optimal dispersions

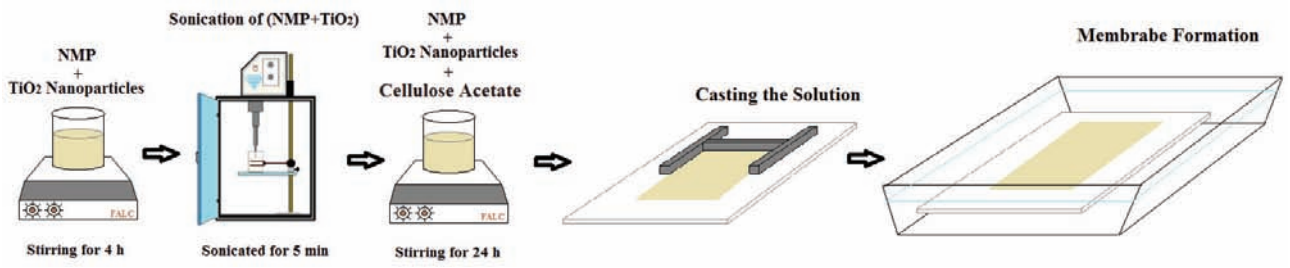

Figure 1. Membrane formation process.

Table 1. Solution compositions and CBTs of each membrane

Membrane code	Solvent (mass%) NMP	Polymer content (17.5 mass%)		CBT, °C
		CA	TiO_2	
M1	82.5	100	0	25
M2		100	0	50
M3		100	0	75
M4		95	5	25
M5		95	5	50
M6		95	5	75
M7		90	10	25
M8		90	10	50
M9		90	10	75
M10		85	15	25
M11		85	15	50
M12		85	15	75
M13		80	20	25
M14		80	20	50
M15		80	20	75
M16		75	25	25
M17		75	25	50
M18		75	25	75

of the particles in the polymer solutions, agitation was required for at least 24 h. The casting solutions were then kept for 24 h to remove air bubbles. After that the casting solutions were cast on a glass plate using a film applicator in a thickness of 200 μm. The cast films were subsequently immersed in a distilled water in 25, 50 and 75 °C baths to complete the phase separation, where exchange between the solvent (NMP) and the non-solvent (distilled water) was induced. Finally, the membranes were heat-treated in a de-ionized water bath at 50 °C for 20 min to remove the excess NMP. The synthesized membranes were kept in a container of de-ionized water to be ready for characterization.

Size analysis of TiO_2 nanoparticles

For analyzing the particle size of TiO_2, a particle size analyzer (SALD-2101) was used. The size of TiO_2 nanoparticles was also investigated by transmission electron microscopy using a PHILIPSEM208S-100KV TEM.

Membrane characterization

Scanning electron microscopy (SEM)

The membranes were snapped under liquid nitrogen to give a generally consistent and clean cut. The membranes were then sputter-coated with thin film of gold and mounted on brass plates with double-sided adhesive tape in a lateral position. Cross-sectional images of the membranes were obtained with a CamScan SEM model MV2300 microscope.

XRD Analysis

For CA membrane, CA/TiO_2 nanocomposite membrane and TiO_2 nanoparticles, X-ray diffraction patterns were obtained with an X-ray diffractometer (D/max-rB 12 kW Rigaku, Japan; 45 kV, 40 mA) operated at 50 mA and 50 kV from 108 to 808.

Thermal gravimetric analysis (TGA)

The thermal degradation was conducted by thermal gravimetric analysis (TGA-50, shimadzu). 25 mg of sample was loaded in a pre-tarred platinum pan and pre-heated above 120 °C to remove moisture. After cooling, the sample was reheated from 25 to 700 °C at a rate of 10 °C/min.

Water content (WC)

Water content of the membranes was obtained after soaking membranes in water for 24 h and the membranes were weighed followed by mopping it with blotting paper. The wet membranes were placed in vacuum drier at 75 °C for 48 h and the dry weights of the membranes were determined [35]. The percent of water content was calculated using the equation:

$$WC\% = \frac{\left(W_{wet} - W_{dry}\right)}{W_{wet}} \times 100 \quad (1)$$

Membrane porosity

Membrane porosity was measured in the method of dry-wet weight, which was determined according to a procedure reported by Chen *et al.* [36]. The porosity ε (%) of the membranes was determined according to Eq. (2) [37]:

$$\varepsilon\% = \frac{\left(W_{wet} - W_{dry}\right)/\rho_{water}}{\left(W_{wet} - W_{dry}\right)/\rho_{water} + W_{dry}/\rho_{water}} \times 100 \quad (2)$$

Pure water flux (PWF)

The PWF measurement was carried out in a batch mode. A flat-sheet membrane module made from stainless steel was used in the experiments. The effective area of the membrane in the module was 39 cm^2. The schematic representation of the setup is shown in Figure 2. PWF experiments were run at a transmembrane pressure of 1 bar with the following equation:

$$PWF = \frac{Q}{A\Delta T} \quad (3)$$

where Q is the quantity of the permeate (L), A is the membrane area (m^2), and Δt is the sampling time (h).

Membrane mean pore diameter

The membrane mean pore diameters were measured by the water flow rate method. The mean pore diameter of the total membrane was calculated by the following equation:

$$r = \sqrt{\frac{(2.9 - 1.75\varepsilon) \times 8\eta l J}{\varepsilon A \Delta P}} \quad (4)$$

where ε is the membrane porosity (%), l is the membrane thickness (m), η is water viscosity (Pa s), J is the pure water flux (m^3/s), A is the effective membrane area (m^2) and ΔP is the transmembrane pressure (Pa).

RESULTS AND DISCUSSION

Size analysis of TiO_2 nanoparticles

The result of the particle size analyzer evaluation of the TiO_2 nanoparticles is shown in Figure 3a. A mixture of distilled water and ethanol (80 mass% H_2O + 20 mass% CH_3CH_2OH) used as a solvent for the determination of particle size distribution. As Figure 3a shows, the average particle size of TiO_2 was equal to 62 nm. Transmission electron microscopy (TEM) was

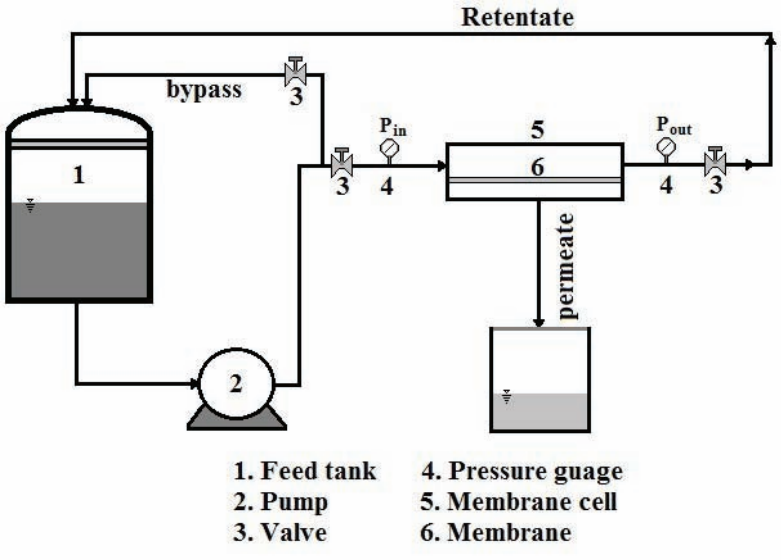

Figure 2. Schematic diagram of the experimental setup.

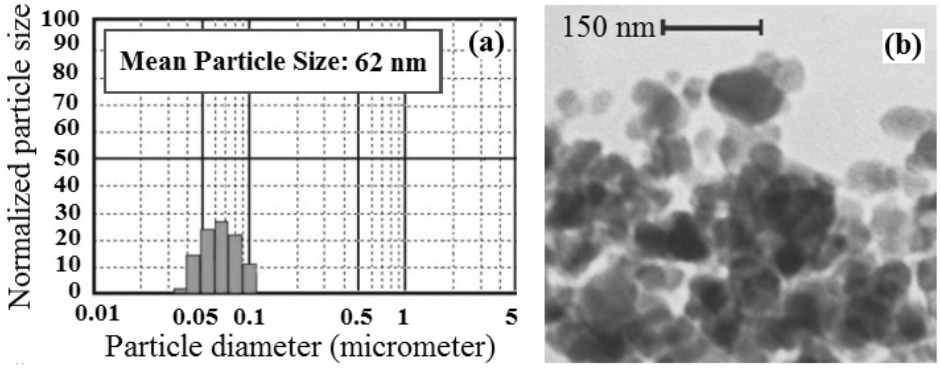

Figure 3. a) Particle size distribution and b) TEM image for TiO_2 nanoparticle produced sonochemically.

used to investigate the particle size of sonochemical synthesized TiO_2 nanoparticles and the result is shown in Figure 3b. The TiO_2 nanoparticles can be seen in the form of black spots and the size are about different from 20 to 140 nm. As this figure shows the average particle size of TiO_2 is equal to 62 nm.

Effect of TiO_2 nanoparticles on membrane morphology

SEM images were taken to determine the effects of the TiO_2 nanoparticles concentration on the membrane morphology. Figures 4 and 5 depict the SEM cross-sectional images of the membranes.

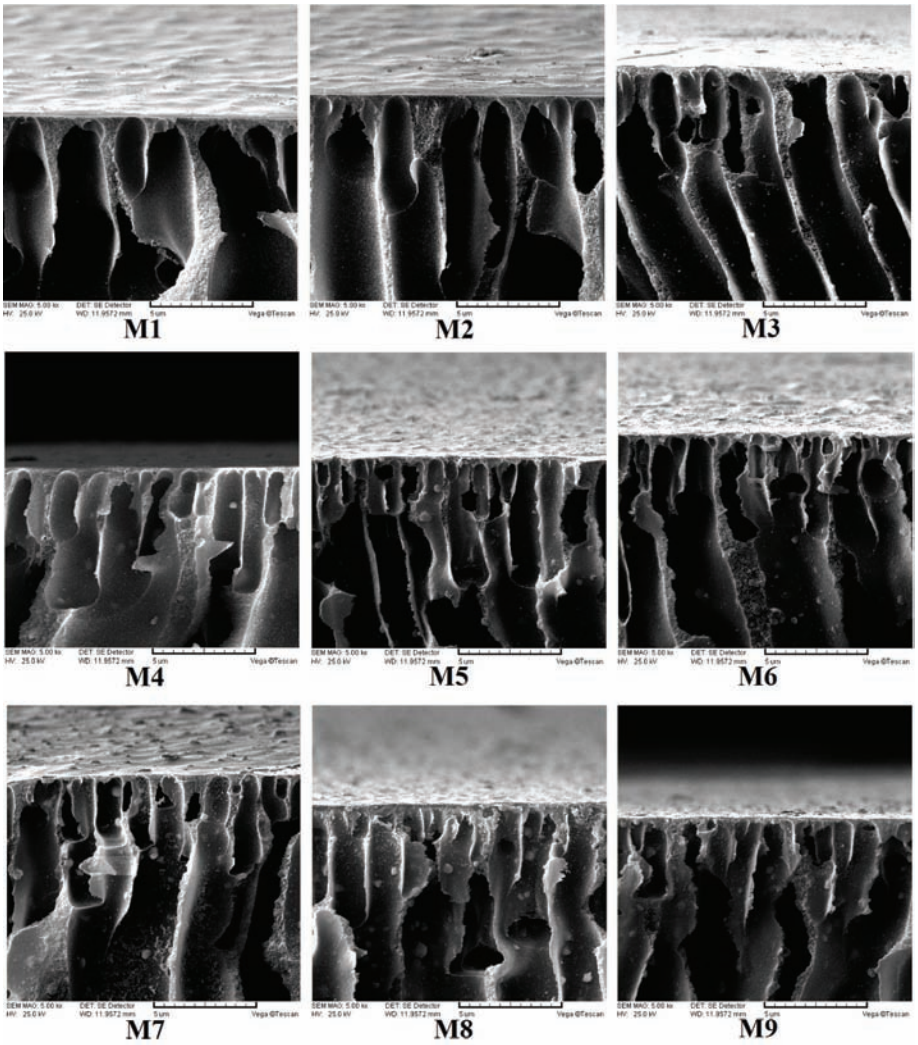

Figure 4. SEM Cross-sectional images of the CA and CA/TiO_2 membranes (M1-M9).

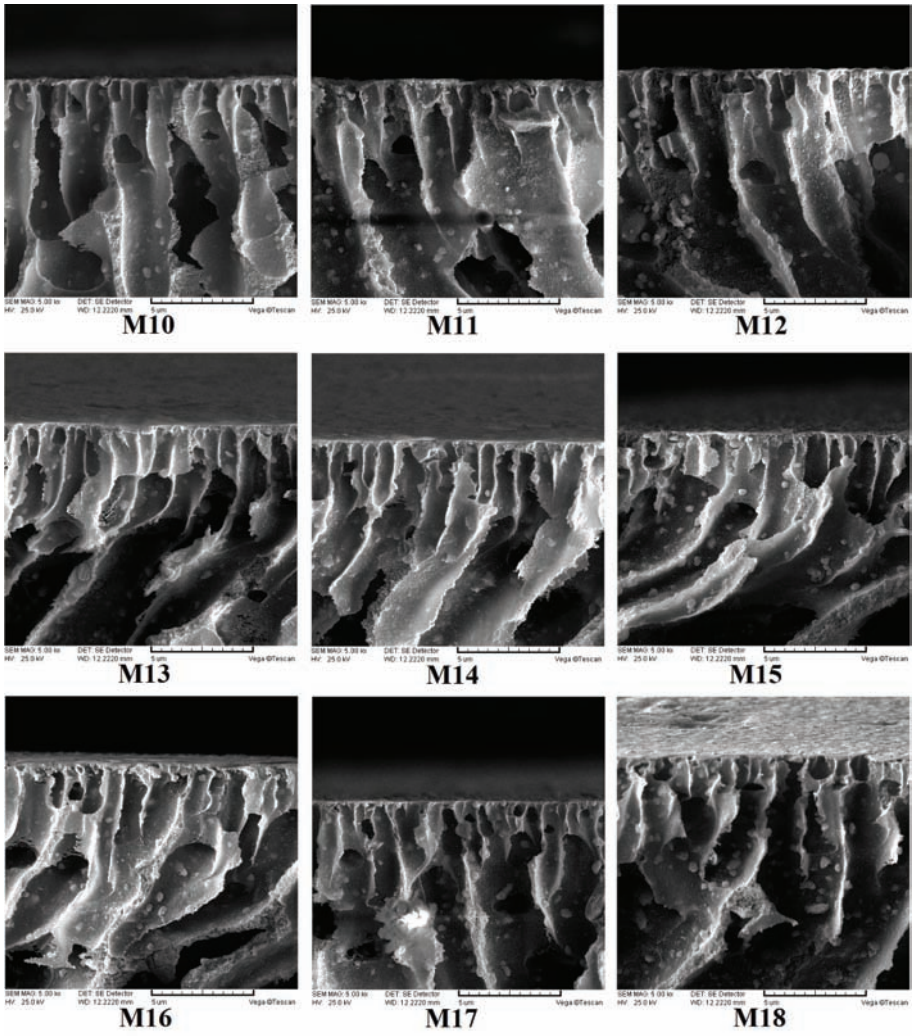

Figure 5. SEM Cross-sectional images of the CA/TiO_2 membranes (M10-M18).

Small addition of TiO_2 nanoparticles to the casting solution resulted in the formation of membrane with denser structure. However, higher concentration of nanoparticles, *i.e.*, 20 and 25 mass% resulted in greater formation of macrovoids and more porous structure. When the cast film was immersed in the distilled water bath, precipitation started because of the low miscibility between the polymer (CA) and the nonsolvent (water). Simultaneously, the miscibility between the solvent (NMP) and the nonsolvent (water) caused diffusional flow of the solvent and nonsolvent (exchange of solvent and nonsolvent) in several points of the film top layer and the substrate, which subsequently led to the formation of nuclei of the polymer phase. In fact, the low affinity between the CA chains and water molecules at points where the water molecules diffused resulted in the repelling of the CA chains and, consequently, the formation of nuclei of the polymer phase. Because of the continuation of the diffusional flow of solvent from the surrounding cast film, these nuclei continued to grow until the polymer concentration at their boundaries became so high that solidification occurred (the demixing process was completed) [38].

The rate of the demixing process affects the membranes morphology. Instantaneous demixing often leads to the formation of macrovoids in membrane structure, whereas slow demixing results in denser structures. In the case of slow demixing, nucleation occurs after a certain period of time, and the polymer concentration increases in the top layer. Then, nucleation starts in the inferior layer at short time intervals successively. Hence, the size and composition of nuclei in the former layer is such that new nuclei are gradually formed in their neighborhood [39]. In other words, in slow demixing, free growth of limited nuclei (on the top layer) is prevented, and a large number of small nuclei is created and distributed throughout the polymer film. Consequently, contrary to instantaneous

demixing, the formation of macrovoids is suppressed, and denser membranes are synthesized.

In this study, the presence of TiO_2 nanoparticles as a hydrophilic additive with nonsolvent properties [40] increased the thermodynamic instability of the cast film and, consequently, led to instantaneous demixing in the coagulation bath and, thus, to the formation of macrovoids in the membrane structure [41]. Hence, the addition of hydrophilic TiO_2 nanoparticles caused greater formation of macrovoids and more porous structures. The effect of TiO_2 nanoparticles on the structure of two prepared membranes is shown in Figure 6. This figure shows the structure differences due to the addition of TiO_2 nanoparticles from 15 to 20 and 25 mass%, in particular, macrovoids size and membrane thickness are more obvious.

Effect of CBT on membrane morphology

As mentioned, SEM images were taken in order to explain the effects of TiO_2 nanoparticles and CBT on the membrane morphology. According to Figure 7, it can be observed that at constant TiO_2 nanoparticles concentration (5 mass%), increasing CBT causes formation of macrovoids and more porous structures. Reduction of CBT (particularly to 25 °C) slows down growth of limited nuclei formed after immersion of the cast film into the coagulation bath. This tranquil growth of primary nuclei, results in formation of numerous nuclei in the cast film. The higher number of nuclei along with intensive reduction of the nuclei growth rate results in suppression of macrovoids and approximately formation of denser structures. These observations are in agreement with the literature [42,43]. In general, it can be said that formation of macrovoids occurs during quick precipitation and the precipitation is faster at higher temperatures. Figure 8 depicts the changes in membranes thickness due to addition of TiO_2 nanoparticles and increasing of CBT.

XRD Analysis

The XRD diffraction patterns of nano-sized TiO_2 particles, CA/TiO_2 nanocomposite membrane and CA membrane were shown in Figure 9. It can be observed that the pattern of TiO_2 nanoparticles had three crystalline characteristic peaks at 2θ of 25.37, 38.43 and 49.61, which correspond to anatase, rutile and brookite respectively. Between three crystalline structures of TiO_2 nanoparticles, the anatase has been reported as a good stabilization and hydrophilicity agent and it is suitable for membrane modification [44]. Figure 9 shows the characteristic peaks of the synthesized TiO_2 nanoparticle located at 25.37° which is close to the literature reported data 25.24° of anatase [44]. It is confirmed that the synthesized TiO_2 nano-

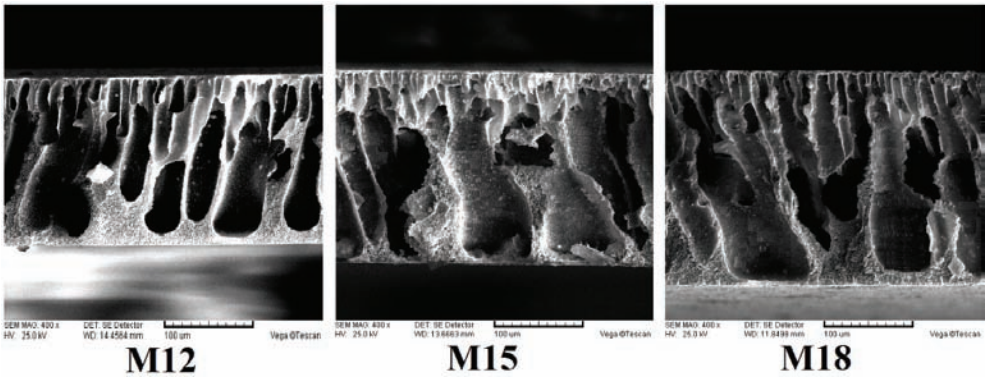

Figure 6. Effect of TiO_2 nanoparticles on porosity and thickness of the M12, M15 and M18 membranes.

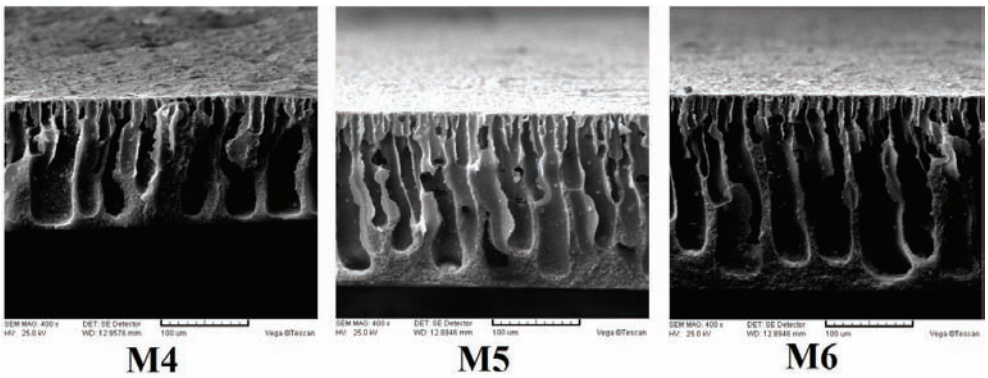

Figure 7. Effect of CBT on porosity and thickness of the M4, M5 and M6 membranes.

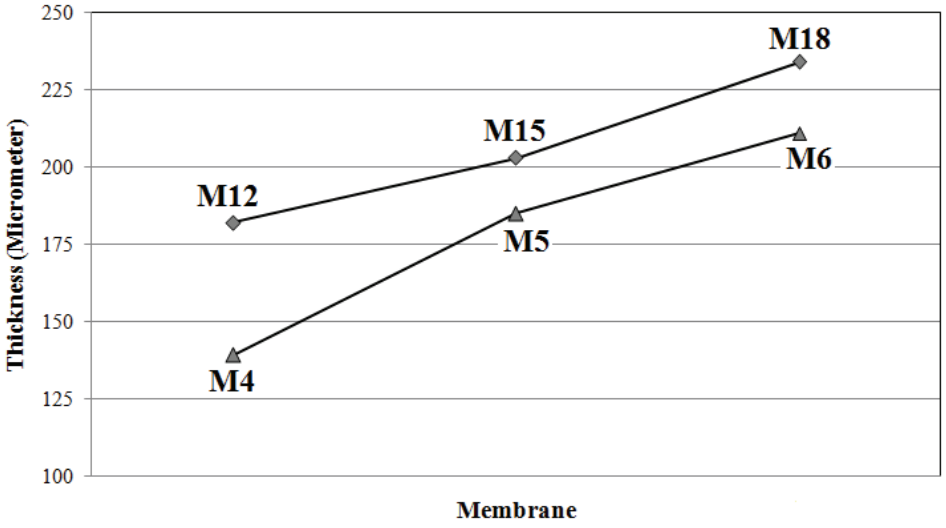

Figure 8. Effect of TiO_2 concentration and CBT on thickness of the membranes.

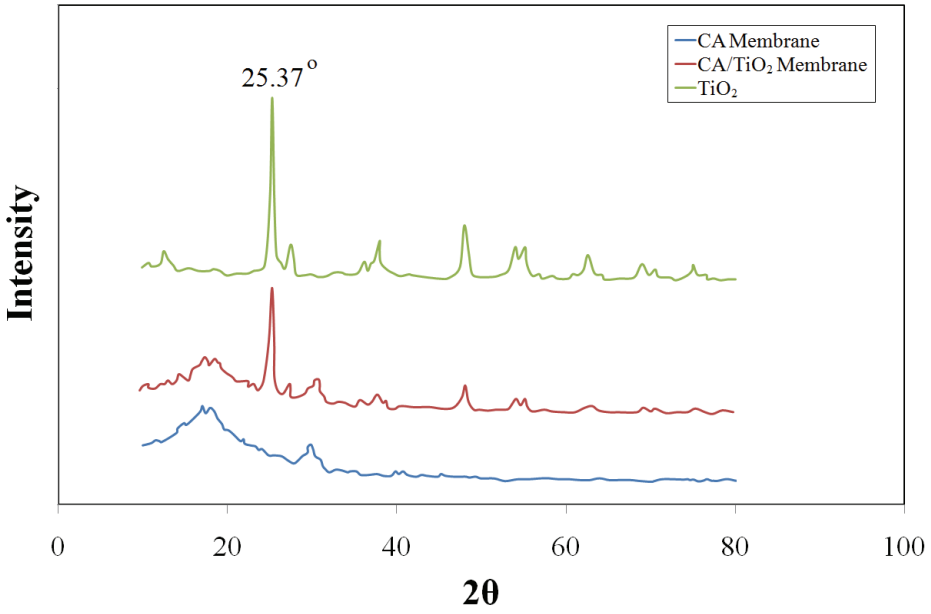

Figure 9. X-Ray diffraction patterns of TiO_2 powder, CA/TiO_2 nanocomposite membrane (with 20 mass% TiO_2) and CA membrane.

particles are mainly composed of anatase, which promises excellent stability, hydrophilicity and anti-fouling characters. The pattern of CA/TiO_2 nanocomposite membrane also had the three crystalline characteristic peaks in addition to the dispersion peak of amorphous CA membrane though the peak locations showed a little shift. It indicated that the nano-sized TiO_2 has distributed to the membrane matrix and there possibly also existed interaction between TiO_2 and CA.

Effect of TiO_2 nanoparticles and CBT on thermal stability of the prepared membranes

The thermal analysis results of the pure CA and CA/TiO_2 nanocomposite membranes are illustrated in Figure 10. It was found that the decomposition temperature (T_d, defined as the temperature at 3% weight loss) was increased with increasing TiO_2 amount. These results confirm that: there is a good compatibility between the TiO_2 nanoparticles and CA; the interaction between TiO_2 nanoparticles and CA increased the rigidity of polymer chain, which enhanced the energy of breaking down the polymer chain; this interaction is due to the covalent bonds between TiO_2 nanoparticles and CA chains.

With increasing TiO_2 content, more heat was absorbed by the TiO_2 in the membranes during heating. This results in the decomposition of delay CA.

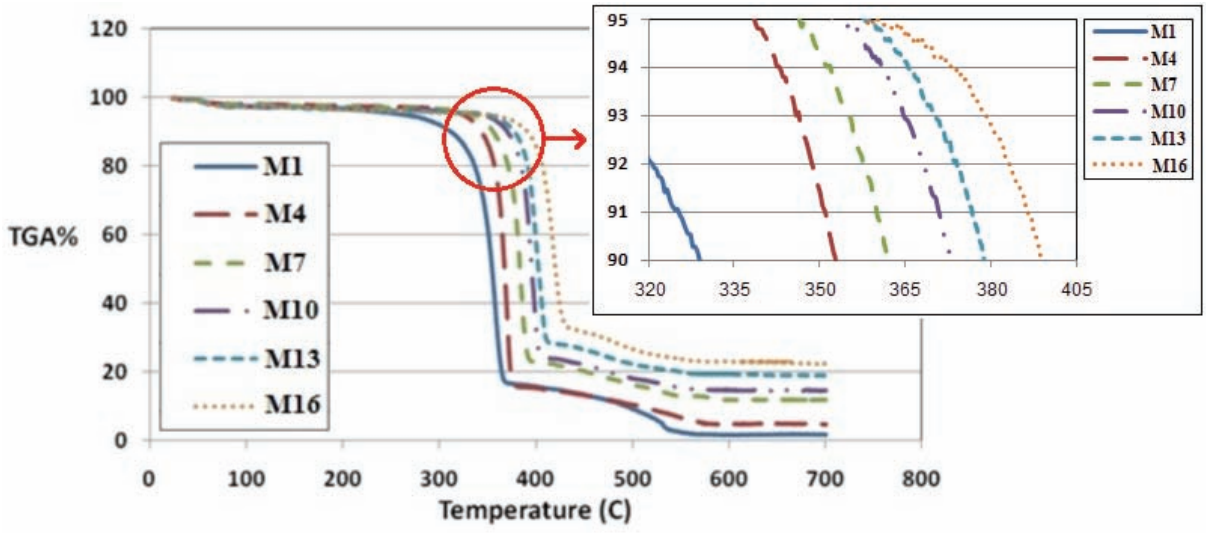

Figure 10. TGA curves of pure CA and CA/TiO_2 nanocomposite membranes.

TGA results also indicated that increasing in CBT leads to the decreasing of decomposition temperature (T_d) of prepared membranes. According to the mechanism of membrane formation, decreasing in CBT caused the sequestration process to happen slower and this lead to smaller thickness of formed membrane. This means that the resulting membrane has more compact polymer chains and more interconnected structure. So with such a membrane structure, greater thermal stability is entitled. According to these descriptions, membranes formed in CBT of 25 °C are more stable than those formed at 50 and 75 °C. As shown in Figure 11, for all prepared membranes, increasing CBT caused the decomposition temperature of polymer chains to decrease.

Water content and membrane porosity

Water content is related to the membrane hydrophilic property [43]. Water content of each membrane is calculated using Eq. (1). As Figure 12 shows, it is obvious that water content is increased by increasing the weight percent of TiO_2 nanoparticles and CBT. In addition of macrovoid formation, separation of polymer chains due to the presence of TiO_2 nanoparticles creates spaces in the polymer matrix, which leads to increasing the water content.

The effect of TiO_2 loading on porosity of nanocomposite membrane was investigated. The porosity of CA and CA/TiO_2 nanocomposite membranes is shown in Table 2. As can be seen, the porosity of membranes slightly increases by increasing the TiO_2 loading in the CA matrix. The reason for this is related to the presence of TiO_2 nanoparticles that increase both porosity and absorption capability of CA/TiO_2 nanocomposite membranes.

Effect of TiO_2 nanoparticles and CBT on Pure Water Flux (PWF)

Figure 13 reveals the effect of TiO_2 nanoparticles concentration and CBT on pure water flux of the membranes prepared from CA/TiO_2/NMP system in water coagulation bath at transmembrane pressure of 1 bar. As observed in Figure 13, addition of TiO_2 nanoparticles to the casting solution results in an incensement in PWF of the prepared membranes. Addition of TiO_2 nanoparticles to the casting solution increases porosity of the membrane support layer and this result in higher PWF. High sub-layer porosity of the membranes prepared from different concentrations of TiO_2 nanoparticles as nanofiller additive in the casting solution, especially at 20 mass%, can be responsible for high performance (higher flux) of the membranes. At 25 mass% of TiO_2 nanoparticles, the aggregation of TiO_2 nanoparticles on the membrane top layer leads to the little decrease of PWF. At constant TiO_2 nanoparticles concentration, PWF increased with the increase of CBT. These measurements confirm the trends observed in the SEM images (Figure 7), where increase in the CBT led to increases in the macrovoid formation and film porosity and, therefore, higher PWF values behavior. As mentioned before, a decrease in the CBT levels intensively reduces the membrane porosity and causes denser structures in the top layer and the sublayer. Thus, a decrease in PWF at lower CBTs is expected. The some cases of PWF results were compared by the other works and presented in Table 3. After determination of PWF and using Eq. (4), the mean pore diameter of each membrane was calculated. Table 2 reveals the changes in mean pore diameter of membranes due to the addition of TiO_2 nanoparticles and increasing in CBT. However, the

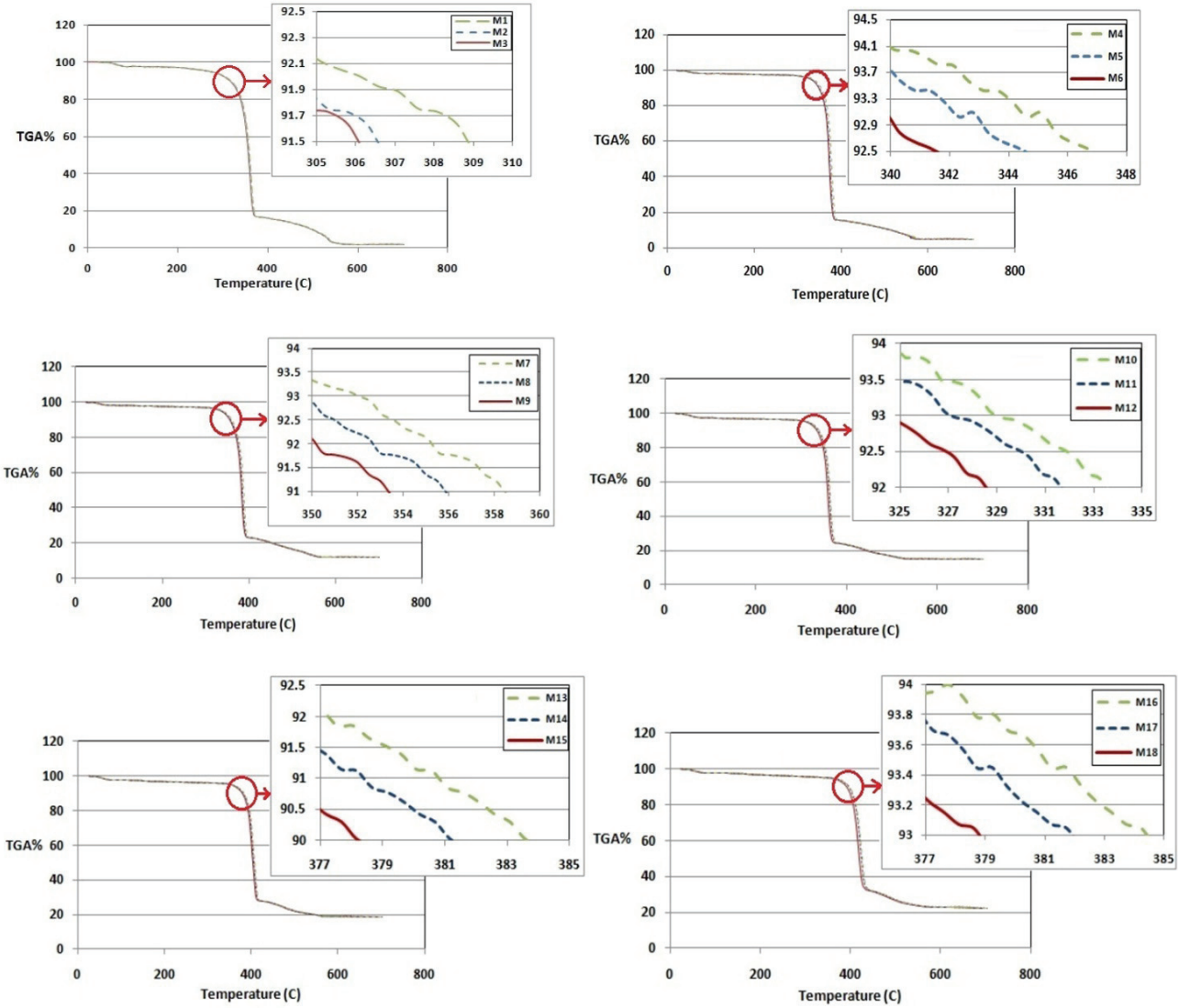

Figure 11. Effect of CBT on decomposition temperature of each membrane.

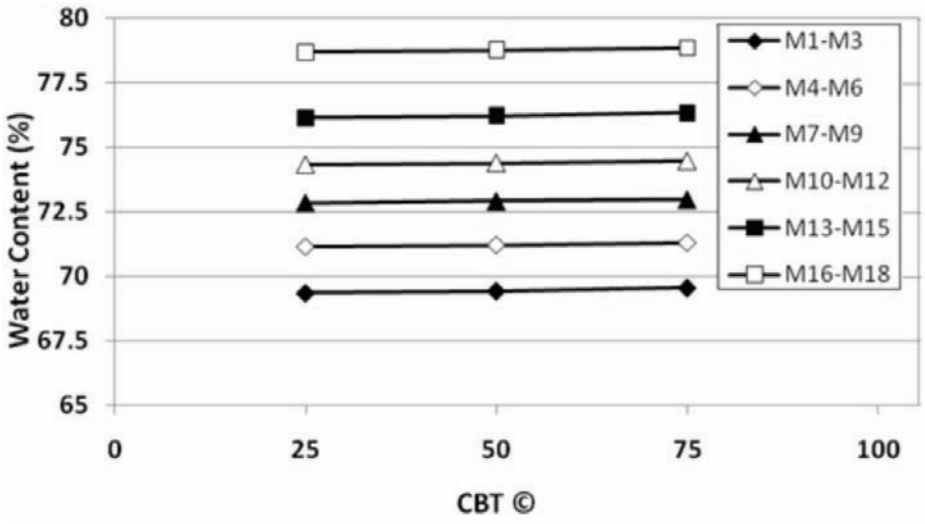

Figure 12. Water content percent of each prepared membranes.

Table 2. Porosity and mean pore diameter of CA and CA/TiO_2 nanocomposite membranes

Membrane code	Porosity, %	Mean pore diameter, nm
M1	69.28 ±0.12	28.3±0.1
M2	69.76±0.11	28.5±0.2
M3	70.14±0.13	28.5±0.1
M4	71.12±0.12	30.2±0.1
M5	71.57±0.15	30.4±0.3
M6	71.92±0.09	30.5±0.2
M7	72.87±0.11	31.1±0.3
M8	73.04±0.10	31.1±0.3
M9	73.43±0.13	31.2±0.4
M10	74.650.14	32.4±0.2
M11	74.86±0.13	32.5±0.1
M12	75.08±0.12	32.7±0.2
M13	76.14±0.08	33.8±0.1
M14	76.43±0.11	33.8±0.4
M15	76.78±0.13	34.0±0.2
M16	78.24±0.12	34.5±0.4
M17	78.63±0.11	34.5±0.1
M18	78.87±0.10	34.7±0.3

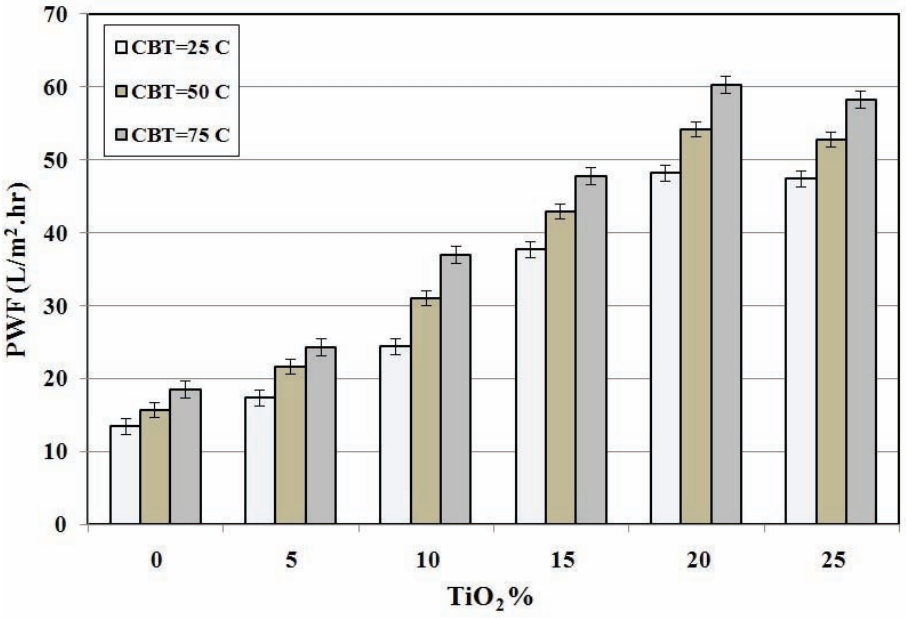

Figure 13. Effect of TiO_2 nanoparticles concentration and CBT on PWF of the prepared membranes.

Table 3. Comparison of pure water permeability of different CA membranes

Composition of the different prepared membranes				Parameter	
CA content, mass%	Additive (Type/mass%)	Solvent	CBT, °C	PWF, L/m^2 h	Ref.
Pure CA	-	NMP	25	10.2	[38]
15.5	PVP/6	NMP	25	39.0	[45]
15.5	PVP/6	NMP	50	10.1	[45]
15.5	PEG/5	NMP	0	84.9	[46]
Pure CA	-	DMF	25	15.6	[47]
17.5	SiO_2/20	DMF	50	42.0	[47]

Table 3. Continued

Composition of the different prepared membranes				Parameter	
CA content, mass%	Additive (Type/mass%)	Solvent	CBT, °C	PWF, L/m^2 h	Ref.
17.5	SiO_2/40	DMF	50	46.7	[47]
Pure CA	-	NMP	25	12.2	[48]
12	Al_2O_3/10	DMF	20	22.3	[49]
Pure CA	-	NMP	75	18.4	This study
17.5	TiO_2/10	NMP	75	38.1	This study
17.5	TiO_2/20	NMP	75	61.2	This study

structure of the membranes were different with the increase of TiO_2 content, the higher TiO_2 content (25 mass%) induced a slight aggregation phenomenon, and produced a considerable number of broken and collapsed pores mostly formed in the vicinity of TiO_2 aggregates in membrane cross section. The defective pore structure originated from the interfacial stresses between polymer and TiO_2 during the membrane drying process when the TiO_2 content was higher. During the drying, the shrinkage rates of the membrane and TiO_2 were different, so the pores morphologies and the membrane interior were destroyed, resulting in broken and collapsed pores.

CONCLUSIONS

Pure CA and CA/TiO_2 nanocomposite membranes were prepared *via* phase inversion by dispersing the TiO_2 nanoparticles, which were synthesized by sonochemical method, in the CA casting solution. Addition of TiO_2 nanoparticles and increasing in CBT resulted in considerable effects on membrane properties. Increasing of TiO_2 nanoparticles concentration in the cast film and CBT resulted in the facilitation of macrovoid formation in the membranes, which increases WC and PWF. TGA analysis showed that CA/TiO_2 nanocomposite membranes had better thermal stability than the pure CA membrane and also by decreasing CBT, greater thermal stability is entitled. PWF of the nanocomposite membranes also improved greatly as the membranes had a more porous structure in addition to the better hydrophilicity. Also like TiO_2 nanoparticles concentration, increasing of CBT led to the permeation enhancing of prepared membranes.

Symbols

W_{wet} Weight of the wet membranes (g)
W_{dry} Weight of the dry membranes (g)
Q Quantity of permeate (L)
A Effective membrane area (m^2)
t Permeation time (h)
ε Membrane porosity
r Membrane mean pore diameter (m)
ρ Water density (kg/m^3)
η Water viscosity (Pa s)
ΔP Transmembrane pressure (Pa)
l Membrane thickness (m)
J Pure water flux (m^3/s)

Abbreviations

TEM Transmission electron microscopy
SEM Scanning electron microscopy
TGA Thermal gravimetric analysis
XRD X-ray diffraction
CBT Coagulation bath temperature (°C)
WC Water content
PWF Pure water flux (L/m^{2}h)

Acknowledgement

Special thanks of the authors go to Research Center of Membrane Processes and Membrane for providing the ultrasonic generator setup and membrane pilot.

REFERENCES

[1] S.M.A. Razavi, S.M. Mousavi, S.A. Mortazavi, Chem. Eng. Sci. **58** (2003) 4185-4195
[2] R. Abedini, A. Mosayebi, Adv. Sustain. Petrol. Eng. Sci. **3** (2011) 15-23
[3] B. Rahmanian, M. Pakizeh, S.A.A. Mansoori, R. Abedini, J. Hazard. Mater. **187** (2011) 67-74
[4] M. Koolivand Salooki, R. Abedini, H. Adib, H. Koolivand, Sep. Purif. Technol. **82** (2011) 1-9
[5] M. Mulder, M. Mulder, Kluwer Academic Publishers, 1997
[6] M.J. Han, S.T. Nam, J. Membr. Sci. **202** (2002) 55-61
[7] B. Jung, J.K. Yoon, B. Kim, H.W. Rhee, J. Membr. Sci. **243** (2004) 45-57
[8] Y. Liu, G.H. Koops, H. Strathmann, J. Membr. Sci. **223** (2003) 187-199
[9] W.Y. Chuang, T.H. Young, W.Y. Chiu, C.Y. Lin, Polymer. **41** (2000) 5633-5641
[10] J.H. Kim, K.H. Lee, J. Membr. Sci. **138** (1998) 153-163
[11] H.J. Kim, R.K. Tyagi, A.E. Fouda, K. Ionasson, J. Appl. Polym. Sci. **62** (1996) 621-629

[12] F.A. Van Vught, Doctoral Thesis, University of Twente, 1998

[13] N. Vogrin, C. Stropnik, V. Musil, M. Brumen, J. Membr. Sci. **207** (2002) 139-141

[14] K.I. Chul, L.K. Ho, J. Appl. Polym. Sci. **89** (2003) 2562--2566

[15] T.H. An, R.R. Chyu, W.D. Ming, L.J. Yih, J. Appl. Polym. Sci. **86** (2002) 166-173

[16] S. Kim, M. Marion, B.H. Jeong, E.M.V. Hoek, J. Membr. Sci. **284** (2006) 361-372

[17] L.J. Yih, L.F. Ching, W.C. Chuan, W.D. Ming, J. Membr. Sci. **118** (1996) 49-61

[18] S.H. Kwak, S.H. Kim, Environ. Sci. Technol. **35** (2001) 2388-2394

[19] K.S. Roelofs, T. Hirth, T. Schiestel, J. Membr. Sci. **346** (2010) 215-226

[20] Z.Q. Huang, K. Chen, S.N. Li, X.T. Yin, Z. Zhang, H.T. Xu, J. Membr. Sci. **315** (2008) 164-171

[21] S. Darvishmanesh, A. Buekenhoudt, J. Degreve, B.V. Bruggen, J. Membr. Sci. **334** (2009) 43-49

[22] L. Yan, Y.S. Li, C.B. Xiang, Polymer. **46** (2005) 7701--7706

[23] J.F. Li, Z.L. Xu, H. Yang, L.Y. Yu, M. Liu, Appl. Surf. Sci. **255** (2009) 4725-4732

[24] J. Ahn, W.J. Chung, I. Pinnau , M.D. Guiver, J. Membr. Sci. **314** (2008) 123-133

[25] D.F. Emerich, C.G. Thanos, Exp. Opin. Biol. Ther. **3** (2003) 655-663

[26] C.T. Campbell, S.C. Parker, D.E. Starr, Science **298** (2002) 811-814

[27] R. Abedini, A. Mosayebi, J. Nat. Sci. Sustain. Technol. **6** (2012) 21-27

[28] L. Kavan, M. Gratzel, J. Rathousky, A. Zukal, J. Electrochem. Soc. **143** (1996) 394-400

[29] B. Samuneva, V. Kozhukharqv, C. Trapalis, R. Kranold, J. Mater. Sci. **28** (1993) 2353-2360

[30] K.S. Mazdiyasni, C.T. Lynch, J.S. Smith, J. Am. Ceram. Soc. **48** (1965) 372-375

[31] H. Cheng, J. Ma, L. Qi, Chem. Mater. **7** (1995) 663-671

[32] S.P. Durand, J. Rouviere, C. Guizard, Colloids Surfaces, A **98** (1995) 251-270

[33] Y. Qian, Q. Chen, Z. Chen, C. Fan, G. Zhou, J. Mater. Chem. **3** (1993) 203-205

[34] R. Abedini, S. M. Mousavi, Chem. Ind. Chem. Eng. Q. **18** (2012) 171−178

[35] M. Sivakumar, A.K. Mohansundaram, D. Mohan, K. Balu, R. Rangarajan, J. Appl. Polym. Sci. **67** (1998) 1939-1946

[36] Z.A. Chen, M.C. Deng, Y. Chen, G.H. He, M. Wu, J.D. Wang, J. Membr. Sci. **235** (2004) 73-86

[37] L.Y. Yu, Z.L. Xu, H.M. Shen, H. Yang, J. Membr. Sci. **337** (2009) 257-265

[38] E. Saljoughi, S.M. Mousavi, Sep. Purif. Technol. **90** (2012) 22-30

[39] E. Saljoughi, M. Amirilargani, T. Mohammadi, J. Appl. Polym. Sci. **111** (2009) 2537-2544

[40] J.J. Qin, M.H. Oo, Y.M. Cao, L.S. Lee, Sep. Purif. Technol., **42** (2005) 291-295

[41] R. Abedini, S.M. Mousavi, R. Aminzadeh, Desalination **277** (2011) 40-45

[42] C.A. Smolders, A.J. Reuvers, R.M. Boom, I.M. Wienk, J. Membr. Sci. **73** (1992) 259-275

[43] M. Sivakumar, D. Mohan, R. Rangarajan, J. Membr. Sci. **268** (2006) 208-219

[44] S.H. Kim, S.Y. Kwak, B.H. Sohn, T.H. Park, J. Membr. Sci. **211** (2003) 157-165

[45] E. Saljoughi, T. Mohammadi, Desalination **249** (2009) 850-854

[46] E. Saljoughi, M. Amirilargani, T. Mohammadi, Desalination **262** (2010) 72-78

[47] G. Arthanareeswaran, T.K.S. Devi, M. Raajenthiren, Sep. Purif. Technol. **64** (2008) 38-47

[48] Z. Li, J. Ren, A.G. Fane, D.F. Li, F.S. Wong, J. Membr. Sci. **279** (2006) 601-607

[49] Y. Wang, L. Yang, G. Luo, Y. Dai, Chem. Eng. J. **146** (2009) 6-10.

REZA ABEDINI[1,2]
SEYED MAHMOUD MOUSAVI[2]
REZA AMINZADEH[1,2]

[1]Research Center of Membrane Processes and Membrane, Ferdowsi University of Mashhad, Mashhad, Iran
[2]Department of Chemical Engineering, Faculty of Engineering, Ferdowsi University of Mashhad, Mashhad, Iran

NAUČNI RAD

UTICAJ SONOHEMIJSKI SINTETISANIH TiO_2 NANOČESTICA I TEMPERATURE KOAGULACIJE NA MORFOLOGIJU, TOPLOTNU STABILNOST I FLUKS ČISTE VODE ASIMETRIČNIH CELULOZNO-ACETATNIH NANOKOMPOZITNIH MEMBRANA PRIPREMLJENIH METODOM FAZNE INVERZIJE

U ovom radu pripremljene su asimetrične nanokompozitne membrane od samo CA i CA/TiO_2, korišćenjem fazne inverzije dispergovanjem TiO_2-nanočestica u rastvoru CA indukovanom imerzionom precipitacijom u vodenom kupatilu za koagulaciju. TiO_2 nanočestice, koje su prethodno sintetizovane sonohemijskom metodom, dodate su u rastvoru za livenje u različitim koncentracijama. Proučavan je i diskutovan uticaj koncentracije TiO_2 nanočestica (0., 5, 10, 15, 20 i 25 mas.%) i temperature koagulacije (CBT, 25, 50 i 75 °C) na morfologiju, termičku stabilnost i fluks čiste vode (PWF) pripremljenih membrana. Povećanje koncentracije TiO_2 u filmu rastvora za livanje zajedno sa većom CBT rezultiralo je u povećanju debljine membrane, sadržaju vode (WC), poroznosti membrane i fluksa čiste vode (PWF). Takođe, ovakve promene olakšavaju formiranje makrošupljina. Termalna gravimetrijska analiza (TGA) pokazuje da je termička stabilnost kompozitnih membrana poboljšana dodavanjem TiO_2 nanočestica. Osim toga, TGA rezultati pokazuju da povećanje CBT pri svakoj koncentraciji TiO_2 dovodi do smanjenja dekompozicione temperature (TD) hibridnih membrana.

Ključne reči: nanokompozitne membrane; celulozo-acetat; TiO_2 nanočestice; fazna inverzija; temperatura koagulacije.